HHS Public Access

Author manuscript

Bioconjug Chem. Author manuscript; available in PMC 2016 December 16.

Published in final edited form as:

Bioconjug Chem. 2016 May 18; 27(5): 1227–1235. doi:10.1021/acs.bioconjchem.6b00075.

Utilizing Viral Nanoparticle/Dendron Hybrid Conjugates in Photodynamic Therapy for Dual Delivery to Macrophages and Cancer Cells

Amy M. Wen[†], **Karin L. Lee**[†], **Pengfei Cao**[‡], **Katrina Pangilinan**[‡], **Bradley L. Carpenter**[§], **Patricia Lam**[†], **Frank A. Veliz**[†], **Reza A. Ghiladi**[§], **Rigoberto C. Advincula**[‡], and **Nicole F. Steinmetz**[*,†,‡,∥,⊥,#]

[†]Department of Biomedical Engineering, Case Western Reserve University, Cleveland, Ohio 44106, United States

[‡]Department of Macromolecular Science and Engineering, Case Western Reserve University, Cleveland, Ohio 44106, United States

[∥]Department of Radiology, Case Western Reserve University, Cleveland, Ohio 44106, United States

[⊥]Department of Materials Science and Engineering, Case Western Reserve University, Cleveland, Ohio 44106, United States

[#]Case Comprehensive Cancer Center, Case Western Reserve University, Cleveland, Ohio 44106, United States

[§]Department of Chemistry, North Carolina State University, Raleigh, North Carolina 27695, United States

Abstract

Photodynamic therapy (PDT) is a promising avenue for greater treatment efficacy of highly resistant and aggressive melanoma. Through photosensitizer attachment to nanoparticles, specificity of delivery can be conferred to further reduce potential side effects. While the main focus of PDT is the destruction of cancer cells, additional targeting of tumor-associated macrophages also present in the tumor microenvironment could further enhance treatment by eliminating their role in processes such as invasion, metastasis, and immunosuppression. In this study, we investigated PDT of macrophages and tumor cells through delivery using the natural noninfectious nanoparticle cowpea mosaic virus (CPMV), which has been shown to have specificity for the immunosuppressive subpopulation of macrophages and also targets cancer cells. We further explored conjugation of CPMV/dendron hybrids in order to improve the drug loading capacity of the nanocarrier. Overall, we demonstrated effective elimination of both macrophage

[*]Corresponding Author: nicole.steinmetz@case.edu.

Supporting Information

The Supporting Information is available free of charge on the ACS Publications website at DOI: 10.1021/acs.bioconj-chem.6b00075.
Supplementary figure for NMR characterization of carboxyl dendron (PDF)

The authors declare no competing financial interest.

and tumor cells at low micromolar concentrations of the photosensitizer when delivered with the CPMV bioconjugate, thereby potentially improving melanoma treatment.

Graphical abstract

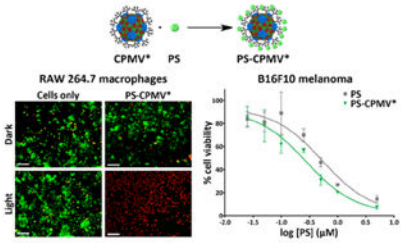

INTRODUCTION

Photodynamic therapy (PDT) is a minimally invasive therapy for the localized treatment of fairly shallow tumors that only requires the presence of a photosensitizer, a light source, and oxygen.[1] The photochemical reaction of light with the photosensitizer results in the formation of reactive oxygen species that induce localized cell killing. Due to spatial control using light application, treatment is limited to a specific area, which can result in fewer systemic effects, greater efficacy, and more cost-effectiveness compared to chemotherapy.[2,3] However, several significant challenges often limit the practical application of PDT, including poor bioavailability and low accumulation in the tumor tissue, dispersal of the photosensitizer throughout the body necessitating avoidance of sunlight for several weeks following treatment, and the hydrophobic nature of most photosensitizers, making them insoluble in physiological conditions.[1,4]

To overcome these challenges, the use of a nanoparticle delivery vehicle for photosensitizers is a potentially advantageous development in PDT due to several benefits, including greater payload delivery that is specific to cancer cells due to both passive and active targeting methods, reduction of toxicity of many hydrophobic photosensitizers that tend to form colloidal aggregates, and prevention of drug inactivation by plasma components.[5] Plant viruses in particular are useful as delivery vehicles due to their ease of manufacture, monodispersity, biocompatibility, and good safety profile.[6] Viruses have been explored for PDT, with applications shown in the treatment of leukemia T cells,[7] prostate cancer cells,[8] and $CD22^{+}$ cells,[9] as well as for antimicrobial therapy.[10]

As a virus-based delivery vehicle for anticancer applications, the 30-nm-sized icosahedron cowpea mosaic virus (CPMV) is particularly noteworthy as it possesses a natural affinity to cancer cells that results from its specificity for and interaction with surface expressed vimentin.[11-13] Furthermore, it has been demonstrated that CPMV has a preference for immune cells, specifically the M2 subpopulation of macrophages, although the mechanism behind this partitioning has not yet been elucidated.[14] The tumor microenvironment is diverse and consists of more than just cancer cells, and macrophages in particular are a major component as well. Whereas the classical M1 macrophages are involved in immune activation and tumor suppression, there is increasing evidence that tumor-associated

macrophages are of an M2 polarization and play a role in the promotion of tumor progression and invasion.[15] The implication of M2 macrophages in suppressing an antitumor immune response makes them a good target for therapy. The elimination of tumor cells together with M2 macrophages has the potential to stimulate the immune system toward destroying any remnant malignant cells.[15,16] Targeting tumor-associated macrophages in general has resulted in greater nanoparticle accumulation and higher efficacy, allowing them to serve as “drug depots” for delivering drugs such as platinum-based chemotherapies to surrounding cancer cells.[17]

A novel photosensitizing drug that has been developed for bactericidal applications,[18-20] and only recently explored for its use in cancer therapy,[21] is a zinc ethynylphenyl porphyrin (Zn-EpPor) photosensitizer (will be referred to as PS). Porphyrin compounds are commonly applied for PDT,[22,23] and the most widely used photosensitizer in the clinic, Photofrin, is composed of porphyrin subunits.[24] PS is unique in that it possesses a positive charge that assists in preferential accumulation in tumor tissue,[25] and its porphyrin ring contains a zinc atom that enhances membrane binding efficiency,[26] both of which makes the photosensitizer more potent.

Thus, the focus of the present paper is to demonstrate the therapeutic efficacy of nanoparticle delivery of PS for the treatment of melanoma, a highly resistant and aggressive cancer where PDT could be applied for greater treatment efficiency.[27] In the process, we established CPMV/dendron hybrids as a platform for expanding particle modification and drug loading capabilities, and also examined the macrophage specificity of CPMV for potential selective delivery. Specifically, we investigated the incorporation of PS into a CPMV-based nanoparticle using electrostatic interactions with anionic generation 3 carboxyl dendrons present on CPMV. Notably, these dendron polymers possess 8 carboxyl groups branching out from a single focal point, which were utilized to enhance the negative charge of the capsid for improved association with the positively charged PS. However, the dendrons also result in an increase in the number of reactive groups displayed on the surface, which could be employed for other applications, such as the attachment of targeting ligands or imaging agents.

Our results with the PS-CPMV conjugate demonstrate a significant improvement in the effective elimination of both macrophage and tumor cells when compared to just the photosensitizer itself, which suggests a wider role for this type of conjugation strategy for improved PDT treatment of cancer.

RESULTS AND DISCUSSION

Design of CPMV-Based Photosensitizer

CPMV was first modified with carboxyl dendrons to impart a greater negative charge, but also with the potential for enhanced functionalizability. CPMV has a highly symmetric structure that is known to atomic scale resolution, and strategies for both interior and exterior chemical conjugation have been established.[28,29] There are 300 lysines displayed in precisely defined arrays on the surface of CPMV that can be targeted. The reaction scheme is shown in Figure 1a. Azide groups were first attached to CPMV using *N*-

hydroxysuccinimide (NHS) ester chemistry to target the lysine residues. Following linker attachment, copper(I)-catalyzed azide–alkyne cycloaddition was used to conjugate an alkyne-functionalized generation 3 dendron with carboxyl groups (see Experimental Procedures and Supporting Information) to the azide-modified CPMV to form a CPMV/dendron hybrid (CPMV*). After dendron attachment, the carboxyl groups now displayed on CPMV were allowed to associate with the cationic Zn-EpPor PS through electrostatic interactions (Figure 1b). Unbound PS was removed by ultracentrifugation, leaving CPMV decorated with PS (PS-CPMV*). Unmodified CPMV was also incubated with PS to compare differences in binding affnity due to the increased charge density.

Characterization of the particles was performed by agarose and SDS gel electrophoresis, transmission electron microscopy (TEM), and UV/visible spectroscopy (Figure 2). Using a native agarose gel, it was observed that conjugation of NHS-azide and carboxyl dendrons both resulted in increased mobility down the gel, as expected. The attachment of the azide to lysine groups on CPMV would result in negation of the positively charged amino acid and faster migration toward the anode. A similar effect was seen for CPMV* due to the negative charge of the carboxyl groups displayed on the dendrons. Additional analysis of carboxyl dendron attachment using an SDS denaturing gel showed successful modification of the coat proteins of CPMV, with additional densities appearing above the unmodified coat protein bands. Density measurements using ImageJ analysis revealed ~45% modification, or 135 out of 300 possible lysines modified and 1080 carboxyl groups introduced from the 8-arm dendrons. Assessment of the particles by TEM showed that the particles remained intact during modification. After utilizing the carboxyl groups for PS incorporation, UV/visible spectroscopy revealed about 200 PS bound to the CPMV* particles compared to 100 per unmodified CPMV. The CPMV capsid has a negative zeta potential,[30] which contributes to the interaction of PS with the wild-type particle. However, the additional negative charge imparted by the dendrons was able to double the PS loading capacity of CPMV. Through visual examination, an advantage of the nanocarrier observed was that the particles remained well dispersed when stored in the fridge over a period of a month, whereas in the same time frame the free PS solution displayed aggregation and sedimentation.

The stability of PS-CPMV* was investigated, with incubation in various solutions explored. The particles were diluted to a concentration of 1 mg/mL and dialyzed against 45 mL of PBS (pH 7) and endolysosomal buffer (pH 5) over a period of 3 days at 37 °C (Figure 3). The endolysosomal buffer was prepared by combining 200 mM citric acid and 200 mM dibasic sodium phosphate buffers such that the final pH was representative of the lysosomal compartment. A slow, almost linear release of PS was observed in PBS buffer, not quite reaching 50% release even after 3 days. On the other hand, a burst release of PS was observed after incubation in the endolysosomal buffer, and 50% release was achieved by around 10 h. The quicker dissociation of PS in the endolysosomal buffer compared to PBS can be attributed to the low pH condition, leading to protonation of the carboxylates and release of the electrostatically coupled PS. Overall, these results are positive, indicating that PS-CPMV* is stable at physiological pH and that low pH can be used to trigger efficient PS dissociation. While beyond the scope of the current study, it will be of interest to further analyze PS-CPMV* stability in vivo. Animal studies will provide insight into the clearance

and biodistribution of the particles, as well as the behavior of the particles in the presence of serum proteins, which will be important considerations for future translation.[31]

Photodynamic Therapy of Macrophages

Uptake of PS-CPMV* and its efficacy for PDT of RAW 264.7 murine macrophages was initially tested using a LIVE/DEAD cell viability assay in a 96-well plate. The macrophages were allowed 8 h to take up either PS-CPMV* at a concentration of 5.0 μM PS or CPMV, CPMV*, and PS controls normalized according to PS or CPMV concentration. After washing, PDT was initialized using a mirror setup where light from a projector was reflected on the cell plate for 30 min. Cells were incubated overnight, then stained with a combination of calcein-AM and ethidium homodimer-1 to detect live and dead cells, respectively (Figures 4a). While cytotoxicity was not observed with the dark controls (Figure 4b), PS-CPMV* and PS were effective at completely eliminating the macrophages, which is quantified in Figure 4c.

Differential attachment and uptake of CPMV was investigated for different macrophage subpopulations of the RAW 264.7 cells. The cells were stimulated with either LPS or IL-4 for polarization toward an M1 or M2 phenotype, respectively, in accordance with previous experiments studying CPMV tropism.[14] Association of CPMV and PS-CPMV* with the cells was then evaluated, with comparison to untreated RAW 264.7 cells as a control. Flow cytometry was performed after 3 h of incubation with the particles (Figure 5a). The presence of CPMV was detected using rabbit anti-CPMV and Alexa Fluor 647-labeled anti-rabbit antibodies, and staining with just the secondary antibody was used as the negative control. Surprisingly, the opposite trend from what was previously reported[14] was observed, with greater presence in M1 macrophages for both CPMV and PS-CPMV* particles. The earlier study utilized Alexa Fluor 488-labeled CPMV particles to measure particle binding and uptake, but also found that addition of a polyethylene glycol (PEG) polymer coating did not change the preference of CPMV for M2 macrophages, so it is unlikely that fluorophore or surface modification would drastically affect the uptake profile.

There is a possibility that the macrophage subpopulations have differences in proteolytic processing and cleavage of the Alexa Fluor 488 from the dye-labeled CPMV, resulting in brighter signal in the M2 subpopulation[32] that we would not observe when using dye-labeled antibodies. There may also be differences in the polarization states between the experiments. To address these issues, additional inclusion of IFN-γ for greater stimulation of M1 polarization and flow cytometry measurements based on PS signal were also investigated. One marker for differentiating macrophage phenotype is their metabolism of arginine.[33] M1 macrophages use nitric oxide synthase (iNOS) to metabolize arginine to citrulline and nitric oxide, while M2 macrophages use arginase-1 (Arg1) for the production of urea, polyamines, and ornithine. Polarization of the macrophages was confirmed using reverse transcription polymerase chain reaction (RT-PCR) to detect relative expression levels of the two genes. RNA was extracted from the stimulated and unstimulated cells, cDNA synthesized, then iNOS- and Arg1-specific primers used for PCR (Figure 5b). There were clear differences in the expression levels of iNOS and Arg1, with higher expression of iNOS for the LPS- and IFN-γ-treated cells and Arg1 expression only observed for cells stimulated with IL-4.

Flow cytometry was again performed using a similar setup as above, except modified to evaluate PS signal in the macrophages rather than using antibody staining (Figure 5c). There was a difference in the fluorescence intensity of the M1 and M2 cells only controls, which was not observed for the first flow cytometry study. The disparity between the two experiments is likely due to differences in the excitation wavelength, since the secondary antibody for CPMV staining is excited at 651 nm and PS is excited at 440 nm. The PS signal was higher in the M1 subpopulation, both for the cells only control and for cells incubated with PS-CPMV*. Due to differences in the background fluorescence, although overall the mean fluorescence intensity was greater for M1 cells, the relative shift in fluorescence was around 325 for both subpopulations, so there is some ambiguity as to whether PS-CPMV* association was greater for the M1 subpopulation. Nevertheless, we can conclusively state that the M2 phenotype was not favored, corroborating data obtained based on the signal from detection of CPMV.

Based on the above results, it is likely that factors other than dye release or insufficient polarization are contributing to the differences observed between the previous and current studies in regard to the affinity of the cells to the PS particles, which will be the subject of further study. For applications in PDT, CPMV specificity for M2 macrophages would be preferable for combination therapy of tumor cells and immunosuppressive macrophages. However, specificity for M1 macrophages could also be utilized for delivery of stimulatory factors that prevent their phenotype switching as well as for aiding in their recruitment of immune cells. The CPMV platform has the additional advantage in terms of immunotherapy due to the fact that it has recently been shown to induce potent antitumor immune response after in situ vaccination in models of skin, ovarian, breast, and colon cancers due to association with and activation of neutrophils.[34] Enhanced efficacy may then be observed from PDT together with the immunostimulatory effect of CPMV.

Photodynamic Therapy of Melanoma

To confirm PDT activity, we evaluated the efficacy of the PS-CPMV* conjugate using the highly aggressive B16F10 melanoma cell line. Uptake of the particles and delivery of PS was first studied using confocal microscopy. B16F10 cells were incubated with PS-CPMV* particles for 3 h, fixed, and stained for the nuclei using 4′,6-diamidino-2-phenylindole (DAPI) and cell membranes using wheat germ agglutinin (WGA). Based on fluorescence signal from the porphyrin, confocal imaging showed that the drug was indeed taken up by the melanoma cells (Figure 6a). Although CPMV is known to be taken up by endocytosis and distributed in punctate patterns throughout the cytoplasm,[32,35] the signal from PS was found to be distributed throughout the cell, including within the nucleus, indicating that the drug gets released from the particles (see Figure 3) and escapes from the endolysosomes.

The distribution of PS throughout the cell is advantageous for PDT. Efficacy was examined using white light therapy of B16F10 cells incubated with CPMV, CPMV*, or PS-CPMV* for 8 h, with concentrations of PS ranging from 0.025 to 5 μM tested. After removal of unbound or noninternalized drug, cell killing was achieved using white light therapy for 30 min, and cell viability was measured using an MTT cell viability assay to assess cell metabolic activity (Figure 6b). A 2-fold improvement in efficacy was achieved with PS-

CPMV* when compared to free PS, with an IC_{50} of 0.28 μM calculated for PS-CPMV* compared to 0.54 μM for PS alone. Toxicity was not observed for cells incubated with CPMV or CPMV* tested at the highest CPMV concentration used for PS-CPMV*, and the dark controls also remained unaffected (data not shown). The low μM IC_{50} of PS-CPMV* is highly effective for PDT and on par with other photosensitizers being evaluated.[36,37] The difference in efficacy between PS and PS-CPMV* could be attributed to more efficient cellular delivery with the nanoparticle.

The advantage of using a nanocarrier is expected to be more profound when applied in vivo, where the nanoparticle would be better able to transport the drug. There have been a number of prior studies that illustrate the well-suited in vivo performance of CPMV. For example, mouse studies have indicated high biocompatibility, as no toxicity was observed even at doses up to 100 mg/kg body weight.[38] Investigations of biodistribution demonstrate standard nanoparticle clearance behavior through mainly the liver and spleen, and quick clearance from tissues was observed only after a few days.[38-40] Additionally, functionalization of CPMV for delivery to cancer cells has been demonstrated with targeting ligands such as bombesin,[41] folic acid,[42] and polyarginine cell penetrating peptides.[43] Therefore, not only does the CPMV platform offer a better solubility profile for PS transport, it also presents the prospect of multimodal formulations that incorporate active targeting for cell-specific delivery.

CONCLUSIONS

In this investigation, we have shown that CPMV/dendron hybrids can be beneficial for introducing greater functionality to the particles. We demonstrated the use of carboxyl dendrons for the increased incorporation of cationic photosensitizers, but the use of dendrons can be applied for a range of other applications, such as enhancement of contrast agent loading and amplification of targeting ligand density. Delivery of the photosensitizer to macrophages was shown to be effective for their elimination. While we were not able to reproduce the previously reported preference of CPMV for the M2 macrophage subpopulation, there were differences in uptake between the M1 and M2 populations observed, and further investigation is warranted. Specificity in targeting one the two subpopulations would be of interest for tuning the delivery of agents to achieve either enhancement of immunostimulatory or elimination of immunosuppressive effects. Overall, PS-CPMV* was found to be effective for PDT of B16F10 melanoma cells, aiding in the delivery of PS. The high efficacy of the Zn-EpPor PS, with an IC_{50} in the low μM range, makes it an attractive candidate for cancer therapy, but the hydrophobicity of the photosensitizer would likely detract from its application in vivo. Using a nanocarrier would be advantageous for reducing undesirable side effects, and the potential for synthesizing a targeted formulation would be a further benefit for carrying this technology forward.

EXPERIMENTAL PROCEDURES

Dendron and Photosensitizer Synthesis

Carboxyl dendrons were synthesized through a ring-opening reaction between succinic anhydride (200 mg, 2.0 mmol) in 5 mL of dried tetrahydrofuran (THF) and a generation 3

polyester-8-hydroxyl-1-acetylene bis-MPA dendron (Sigma, 86.8 mg, 0.1 mmol) in the presence of triethylamine (TEA, 167 mL, 1.2 mmol) and 4-dimethylaminopyridine (DMAP, 48.9 mg, 0.4 mmol) that were dissolved in 10 mL of dried THF. The reaction was stirred for 24 h at 40 °C, the solvent evaporated, and methanol added to dissolve the mixture. The final product was purified by dialysis against methanol using dialysis tubing with a molecular weight cutoff of 100–500 Da. Verification of the product was performed by ^{1}H NMR analysis.

The cationic zinc ethynylphenyl porphyrin photosensitizer (Zn-EpPor PS) used in this study was synthesized based on previously published methods.[19] In brief, the porphyrin was first synthesized under mildly acidic conditions using 4-pyrindinecarboxaldehyde, 4-[(trimethylsilyl)ethynyl]-benzaldehyde, and pyrrole then purified by column chromatography. Ethyne deprotection was accomplished in a 1:4 solution of methanol/THF with potassium carbonate, then zinc acetate in methanol/THF was used for addition of zinc. Finally, iodomethane in dimethylformamide (DMF) at elevated temperatures was used for amine quaternization of the pyridine substituents.

CPMV Purification

CPMV was propagated in *Vigna unguiculata* black-eyed pea plants 10–14 days after planting using mechanical inoculation with a 0.1 mg/mL solution of CPMV. Viral particles were isolated using a combination of blending, chloroform/butanol extraction, and centrifugation based on established methods.[44]

CPMV Modifications

CPMV was first modified with azide linkers using an overnight reaction of 6000 molar excess of *N*-hydroxysuccinimide (NHS)-PEG_4-azide (Thermo Scientific) with a 2 mg/mL concentration of CPMV in 0.1 M potassium phosphate (KP) buffer, pH 7.0 with 10% (v/v) DMSO. Purification was performed by ultracentrifugation pelleting at 42 000 rpm. To further display carboxyl dendrons on CPMV (CPMV*), alkyne-functionalized carboxyl dendrons were attached using 2400 molar excess with 2 mg/mL CPMV-N_3 in 0.1 M KP buffer, pH 7.0 in the presence of 20 mM aminoguanidine, 20 mM L-ascorbic acid, and 2 mM $CuSO_4$ that was added together with 10 mM tris(benzyltriazolylmethyl)-amine (THPTA). 10 kDa molecular weight cutoff centrifugal filters (Millipore) were used to purify the reaction after 2 h at room temperature. Drug-labeled formulations were then made by incubating 1000 molar excess of PS (from 50 mg/mL stock) with CPMV* in 10 mM KP buffer, pH 7.8 overnight, then removing unattached PS by ultracentrifugation pelleting in 0.1 M KP buffer, pH 7.8, which was also the buffer used for resuspension of the particles. Any aggregates were removed by a clearing spin at 10 000 rpm for 10 min before obtaining the final solution.

UV/visible Spectroscopy

CPMV and PS concentrations were determined by UV/visible spectroscopy, with a molar absorptivity coefficient for CPMV of 8.1 mg^{-1} mL cm^{-1} at 260 nm and for PS of 195 000 M^{-1} cm^{-1} at 440 nm.

Gel Electrophoresis

DNA samples were analyzed with 2% (w/v) agarose gels run in TAE buffer at 100 V for 1 h and stained with GelRed nucleic acid stain (Biotium). CPMV samples were analyzed by agarose gel electrophoresis with 1.2% (w/v) agarose gels run in TBE buffer at 100 V for 1 h. CPMV particles were also denatured into individual coat protein subunits by heating for 5 min at 100 °C, then separated on denaturing 4–12% NuPAGE gels (Invitrogen) in MOPS running buffer (Invitrogen). CPMV gels were stained using Coomassie blue, and all gels were photographed using an AlphaImager imaging system (Biosciences).

Transmission Electron Microscopy

Particles were diluted in distilled water and adsorbed to Formvar carbon-coated copper grids at a concentration of 0.1 mg/mL for 5 min. This was followed by a brief wash with distilled water, then negative staining with 2% (w/v) uranyl acetate for 2 min. Imaging was performed using a Zeiss Libra 200FE transmission electron microscope at 200 kV.

LIVE/DEAD Assay

RAW 264.7 macrophages were seeded overnight in 96-well plates, with one plate used as a dark control, at a concentration of 10 000 cells/100 μL Dulbecco's modified Eagle's medium (DMEM, Gibco) supplemented with 10% (v/v) fetal bovine serum (FBS, Atlanta Biologicals) and 1% (v/v) penicillin–streptomycin (pen-strep, Life Technologies). Cells were then incubated for 8 h at 37 °C and 5% CO_2 with triplicates of CPMV, CPMV*, PS-CPMV*, or PS corresponding to 5.0 μM PS or normalized for nanoparticle concentration accordingly. After washing twice with PBS, 100 μL medium was added. Photodynamic therapy was applied using a Vivitek D950HD projector reflected off a mirror to result in a rectangular area (10.5 cm × 11 cm) that corresponded to a dose of about 18.1 J cm^{-2} at 430 nm, and then the cells were returned to the incubator overnight. Treatment with 70% (v/v) methanol for 30 min was used as a control for dead cells. Cell viability was determined using a LIVE/DEAD assay for mammalian cells (Thermo Fisher) following manufacturer's procedures for cell staining and using a Zeiss Axio Observer Z1 motorized FL inverted microscope for imaging. Analysis was performed with ImageJ (http://imagej.nih.gov/ij) to measure percentage cell viability.

Macrophage Cell Polarization

RAW 264.7 macrophages were seeded in 6-well plates at a concentration of 500 000 cells/2 mL DMEM supplemented with 10% (v/v) heat-inactivated FBS and 1% (v/v) pen-strep. After 5 h for growth and adhesion at 37 °C and 5% CO_2, 50 ng/mL of either LPS (Sigma) or IL-4 (Biolegend) was added to the wells for M1 and M2 polarization, respectively, and allowed to stimulate the cells for an additional 24 h. As an additional method for M1 polarization, 50 ng/mL of LPS and 20 ng/mL of IFN-γ (Biolegend) was also evaluated.

Reverse Transcription Polymerase Chain Reaction (RT-PCR)

RNA extraction was carried out using TRI Reagent (Molecular Research Center) according to manufacturer's specifications. cDNA was made using SuperScript VILO Master Mix (Invitrogen) with 500 ng of RNA. DreamTaq PCR Master Mix (Thermo Scientific) was then

used to analyze gene expression of iNOS, arginase-1 (Arg1), and β-actin. 5′-GCCTCATGCCATTGAGTTCATCAACC-3′ and 5′-GAGCTGTGAATTCCAGAGCCTGAAG-3′ were the sense and antisense primers used for iNOS,[45] 5′-CAGAAGAATGGAAGAGTCAG-3′ and 5′-CAGATATGCAGGGAGTCACC-3′ were the sense and antisense primers used for Arg1,[46] and 5′-GGCTGTATTCCCCTCCATCG-3′ and 5′-CCAGTTGGTAACAATGCCATGT-3′ were the sense and antisense primers used for β-actin.[47] Amplification was performed with 2 μL of cDNA diluted 1:10 and 4 pmol of each primer in a 20 μL reaction with the following steps: (1) 2 min at 94 °C; (2) 30 cycles of 94 °C for 30 s, 55 °C for 20 s, 72 °C for 20 s; and (3) 5 min at 72 °C for final extension. Expected product sizes were 372 bp for iNOS, 249 bp for Arg1, and 154 bp for β-actin.

Flow Cytometry

After macrophage polarization (see above), the cells were removed with Hanks'-based cell dissociation buffer (Gibco) and resuspended in sterile PBS. The cells were added to v-bottom 96-well plates at a density of 300 000 cells/200 μL (for PS signal) or 500 000 cells/200 μL (for CPMV antibody staining) and incubated with 100 000 particles/cell for 3 h at 37 °C. The cells were washed twice with FACS buffer (PBS with 1 mM EDTA, 25 mM HEPES, 1% (v/v) FBS, pH 7.0), fixed with 2% (v/v) formaldehyde in FACS buffer for 10 min at room temperature, then washed twice again with FACS buffer. Data obtained based on PS signal were acquired using a BD FACSAria SORP cell sorter gated for 10 000 events. CPMV staining was performed by first briefly permeabilizing the membrane with permeabilization buffer (0.2% saponin in FACS buffer). The cells were incubated at 4 °C for 1 h with primary rabbit anti-CPMV antibody (Pacific Immunology) diluted 1:1000 in permeabilization buffer, washed twice with permeabilization buffer, incubated another hour at 4 °C with Alexa Fluor 647-labeled goat anti-rabbit secondary antibody (Thermo Scientific) diluted 1:2000 in permeabilization buffer, and then washed three times with permeabilization buffer. After the final wash, the cells were resuspended in FACS buffer and analyzed on a BD LSR II flow cytometer, gated for 10 000 events. Data were processed using FlowJo software (Tree Star).

PS Release Assay

To study PS release, PS-CPMV* was incubated in PBS and endolysosomal buffer (28 mL of 200 mM citric acid mixed with 65.5 mL of 200 mM dibasic sodium phosphate, pH 5).[48] 200 μL of 1 mg/mL PS-CPMV* was dialyzed using a Slide-A-Lyzer Mini dialysis unit (10 kDa molecular weight cutoff) in 45 mL of each solution prewarmed to 37 °C. Samples were incubated at 37 °C with shaking (80 rpm). 10 μL of the samples was removed at 1, 3, 8, 24, 48, and 72 h, and the concentration of PS remaining was determined by UV/visible spectroscopy (see above). Analysis was performed using GraphPad Prism.

Confocal Microscopy

Localization of PS after cell uptake of PS-CPMV* in B16F10 melanoma cells was evaluated by confocal microscopy. Cells were seeded on coverslips in untreated 24-well plates at a concentration of 25 000 cells/500 μL DMEM supplemented with 10% (v/v) FBS and 1% (v/v) pen-strep and allowed to grow overnight at 37 °C and 5% CO_2. All steps following

were performed in the dark. PS-CPMV* was added at a concentration of 1×10^7 particles/cell, and then the cells were returned to the incubator for 3 h. Cells were fixed using DPBS containing 4% (v/v) paraformaldehyde and 0.3% (v/v) gluteraldehyde for 10 min at room temperature. After washing 3 times with DPBS, the cells were incubated with 1 μg/mL Alexa Fluor 488-conjugated wheat germ agglutinin (Invitrogen) in DPBS with 5% (v/v) goat serum for 45 min at room temperature. The cells were washed a further 3 times with DPBS, and then the coverslips were mounted onto microscope slides with Fluoroshield with DAPI (Sigma). Imaging was performed using an Olympus FluoView FV1000 confocal microscope and analysis performed with ImageJ.

MTT Cell Viability Assay

B16F10 cells were seeded (2000 cells/100 μL DMEM/well) in a treated 96-well plate overnight at 37 °C and 5% CO_2. Triplicates of PS-CPMV* were added to the cells at concentrations of 0.025, 0.05, 0.1, 0.25, 0.5, 1.0, and 5.0 μM PS. CPMV and CPMV* matching the CPMV concentration for PS-CPMV* at 5.0 μM PS were used as controls, along with cells with no added particles. A dark control for all the samples was also used. The cells were incubated at 37 °C and 5% CO_2 for 8 h to allow for cell binding and uptake. Free particles and PS were washed with PBS and 100 μL of fresh medium added. The cells were then irradiated with white light for 30 min as detailed above with the LIVE/ DEAD assay. The cells were returned to the incubator for 48 h after treatment, and their viability was subsequently measured using an MTT cell proliferation assay kit (ATCC) based on manufacturer's instructions. A Tecan Infinite 200 plate reader was used to measure absorbance at 570 nm, and the percent cell viability was determined by normalizing to the cells only control. Data analysis was performed with GraphPad Prism.

Statistical Analysis

Plots show mean and standard deviation. Student's *t* test was used to determine significance.

Supplementary Material

Refer to Web version on PubMed Central for supplementary material.

Acknowledgments

This work was supported by grants from the National Science Foundation (CMMI NM 333651 to N.F.S. and R.C.A.) and the National Institutes of Health (F31 HL129703 to A.M.W. and T32 EB007509 to K.L.L.).

References

1. Agostinis P, Berg K, Cengel KA, Foster TH, Girotti AW, Gollnick SO, Hahn SM, Hamblin MR, Juzeniene A, Kessel D, et al. Photodynamic therapy of cancer: an update. Ca-Cancer J Clin. 2011; 61:250–281. [PubMed: 21617154]
2. Chen KC, Hsieh YS, Tseng YF, Shieh MJ, Chen JS, Lai HS, Lee JM. Pleural Photodynamic Therapy and Surgery in Lung Cancer and Thymoma Patients with Pleural Spread. PLoS One. 2015; 10:e0133230. [PubMed: 26193470]
3. Kubler A, Niziol C, Sidhu M, Dunne A, Werner JA. Analysis of cost effectiveness of photodynamic therapy with Foscan (Foscan-PDT) in comparison with palliative chemotherapy in patients with

advanced head-neck tumors in Germany. Laryngorhinootologie. 2005; 84:725–732. [PubMed: 16231239]

4. Huang Z, Xu H, Meyers AD, Musani AI, Wang L, Tagg R, Barqawi AB, Chen YK. Photodynamic therapy for treatment of solid tumors–potential and technical challenges. Technol Cancer Res Treat. 2008; 7:309–320. [PubMed: 18642969]
5. Lucky SS, Soo KC, Zhang Y. Nanoparticles in photodynamic therapy. Chem Rev. 2015; 115:1990–2042. [PubMed: 25602130]
6. Manchester M, Singh P. Virus-based nanoparticles (VNPs): platform technologies for diagnostic imaging. Adv Drug Delivery Rev. 2006; 58:1505–1522.
7. Stephanopoulos N, Tong GJ, Hsiao SC, Francis MB. Dual-surface modified virus capsids for targeted delivery of photodynamic agents to cancer cells. ACS Nano. 2010; 4:6014–6020. [PubMed: 20863095]
8. Wen AM, Ryan MJ, Yang AC, Breitenkamp K, Pokorski JK, Steinmetz NF. Photodynamic activity of viral nanoparticles conjugated with C60. Chem Commun (Cambridge, U K). 2012; 48:9044–9046.
9. Rhee JK, Baksh M, Nycholat C, Paulson JC, Kitagishi H, Finn MG. Glycan-targeted virus-like nanoparticles for photodynamic therapy. Biomacromolecules. 2012; 13:2333–2338. [PubMed: 22827531]
10. Suci PA, Varpness Z, Gillitzer E, Douglas T, Young M. Targeting and photodynamic killing of a microbial pathogen using protein cage architectures functionalized with a photosensitizer. Langmuir. 2007; 23:12280–12286. [PubMed: 17949022]
11. Koudelka KJ, Rae CS, Gonzalez MJ, Manchester M. Interaction between a 54-kilodalton mammalian cell surface protein and cowpea mosaic virus. J Virol. 2007; 81:1632–1640. [PubMed: 17121801]
12. Steinmetz NF, Cho CF, Ablack A, Lewis JD, Manchester M. Cowpea mosaic virus nanoparticles target surface vimentin on cancer cells. Nanomedicine. 2011; 6:351–364. [PubMed: 21385137]
13. Koudelka KJ, Destito G, Plummer EM, Trauger SA, Siuzdak G, Manchester M. Endothelial targeting of cowpea mosaic virus (CPMV) via surface vimentin. PLoS Pathog. 2009; 5:e1000417. [PubMed: 19412526]
14. Agrawal A, Manchester M. Differential uptake of chemically modified cowpea mosaic virus nanoparticles in macrophage subpopulations present in inflammatory and tumor microenvironments. Biomacromolecules. 2012; 13:3320–3326. [PubMed: 22963597]
15. Sica A, Schioppa T, Mantovani A, Allavena P. Tumour-associated macrophages are a distinct M2 polarised population promoting tumour progression: potential targets of anti-cancer therapy. Eur J Cancer. 2006; 42:717–727. [PubMed: 16520032]
16. Tang X, Mo C, Wang Y, Wei D, Xiao H. Anti-tumour strategies aiming to target tumour-associated macrophages. Immunology. 2013; 138:93–104. [PubMed: 23113570]
17. Miller MA, Zheng YR, Gadde S, Pfirschke C, Zope H, Engblom C, Kohler RH, Iwamoto Y, Yang KS, Askevold B, et al. Tumour-associated macrophages act as a slow-release reservoir of nano-therapeutic Pt(IV) pro-drug. Nat Commun. 2015; 6:8692. [PubMed: 26503691]
18. Carpenter BL, Feese E, Sadeghifar H, Argyropoulos DS, Ghiladi RA. Porphyrin-cellulose nanocrystals: a photobactericidal material that exhibits broad spectrum antimicrobial activity. Photochem Photobiol. 2012; 88:527–536. [PubMed: 22360680]
19. Feese E, Sadeghifar H, Gracz HS, Argyropoulos DS, Ghiladi RA. Photobactericidal porphyrin-cellulose nanocrystals: synthesis, characterization, and antimicrobial properties. Biomacromolecules. 2011; 12:3528–3539. [PubMed: 21838250]
20. Carpenter BL, Scholle F, Sadeghifar H, Francis AJ, Boltersdorf J, Weare WW, Argyropoulos DS, Maggard PA, Ghiladi RA. Synthesis, Characterization, and Antimicrobial Efficacy of Photomicrobicidal Cellulose Paper. Biomacromolecules. 2015; 16:2482–2492. [PubMed: 26181636]
21. Lee KL, Carpenter BL, Wen AM, Ghiladi RA, Steinmetz NF. High-aspect ratio nanotubes formed by tobacco mosaic virus for delivery of photodynamic agents targeting melanoma. ACS Biomater Sci Eng. 2016; doi: 10.1021/acsbiomaterials.6b00061

22. Liang X, Li X, Jing L, Yue X, Dai Z. Theranostic porphyrin dyad nanoparticles for magnetic resonance imaging guided photodynamic therapy. Biomaterials. 2014; 35:6379–6388. [PubMed: 24818886]
23. Cui L, Lin Q, Jin CS, Jiang W, Huang H, Ding L, Muhanna N, Irish JC, Wang F, Chen J, et al. A PEGylation-Free Biomimetic Porphyrin Nanoplatform for Personalized Cancer Theranostics. ACS Nano. 2015; 9:4484–4495. [PubMed: 25830219]
24. Juarranz A, Jaen P, Sanz-Rodriguez F, Cuevas J, Gonzalez S. Photodynamic therapy of cancer. Basic principles and applications. Clin Transl Oncol. 2008; 10:148–154. [PubMed: 18321817]
25. Jensen TJ, Vicente MG, Luguya R, Norton J, Fronczek FR, Smith KM. Effect of overall charge and charge distribution on cellular uptake, distribution and phototoxicity of cationic porphyrins in HEp2 cells. J Photochem Photobiol, B. 2010; 100:100–111. [PubMed: 20558079]
26. Pavani C, Uchoa AF, Oliveira CS, Iamamoto Y, Baptista MS. Effect of zinc insertion and hydrophobicity on the membrane interactions and PDT activity of porphyrin photosensitizers. Photochem Photobiol Sci. 2009; 8:233–240. [PubMed: 19247516]
27. Baldea I, Filip AG. Photodynamic therapy in melanoma–an update. J Physiol Pharmacol. 2012; 63:109–118. [PubMed: 22653896]
28. Wen AM, Shukla S, Saxena P, Aljabali AA, Yildiz I, Dey S, Mealy JE, Yang AC, Evans DJ, Lomonossoff GP, et al. Interior engineering of a viral nanoparticle and its tumor homing properties. Biomacromolecules. 2012; 13:3990–4001. [PubMed: 23121655]
29. Wang Q, Kaltgrad E, Lin T, Johnson JE, Finn MG. Natural supramolecular building blocks: Wild-type cowpea mosaic virus. Chem Biol. 2002; 9:805–811. [PubMed: 12144924]
30. Aljabali AA, Evans DJ. Templated mineralization by charge-modified cowpea mosaic virus. Methods Mol Biol. 2014; 1108:89–95. [PubMed: 24243242]
31. Pitek AS, Wen AM, Shukla S, Steinmetz NF. The Protein Corona of Plant Virus Nanoparticles Influences their Dispersion Properties, Cellular Interactions, and In Vivo Fates. Small. 2016; 12:1758–1769. [PubMed: 26853911]
32. Wen AM, Infusino M, De Luca A, Kernan DL, Czapar AE, Strangi G, Steinmetz NF. Interface of physics and biology: engineering virus-based nanoparticles for biophotonics. Bioconjugate Chem. 2015; 26:51–62.
33. Galvan-Pena S, O'Neill LA. Metabolic reprograming in macrophage polarization. Front Immunol. 2014; 5:420. [PubMed: 25228902]
34. Lizotte PH, Wen AM, Sheen MR, Fields J, Rojanasopondist P, Steinmetz NF, Fiering S. In situ vaccination with cowpea mosaic virus nanoparticles suppresses metastatic cancer. Nat Nanotechnol. 2015; 11:295. [PubMed: 26689376]
35. Plummer EM, Manchester M. Endocytic uptake pathways utilized by CPMV nanoparticles. Mol Pharmaceutics. 2013; 10:26–32.
36. Rangasamy S, Ju H, Um S, Oh DC, Song JM. Mitochondria and DNA Targeting of 5,10,15,20-Tetrakis(7-sulfonatobenzo[b]thiophene) Porphyrin-Induced Photodynamic Therapy via Intrinsic and Extrinsic Apoptotic Cell Death. J Med Chem. 2015; 58:6864–6874. [PubMed: 26295496]
37. Tachikawa S, El-Zaria ME, Inomata R, Sato S, Nakamura H. Synthesis of protoporphyrin-lipids and biological evaluation of micelles and liposomes. Bioorg Med Chem. 2014; 22:4745–4751. [PubMed: 25066052]
38. Singh P, Prasuhn D, Yeh RM, Destito G, Rae CS, Osborn K, Finn MG, Manchester M. Bio-distribution, toxicity and pathology of cowpea mosaic virus nanoparticles in vivo. J Controlled Release. 2007; 120:41–50.
39. Rae CS, Khor IW, Wang Q, Destito G, Gonzalez MJ, Singh P, Thomas DM, Estrada MN, Powell E, Finn MG, et al. Systemic trafficking of plant virus nanoparticles in mice via the oral route. Virology. 2005; 343:224–235. [PubMed: 16185741]
40. Shukla S, Ablack AL, Wen AM, Lee KL, Lewis JD, Steinmetz NF. Increased tumor homing and tissue penetration of the filamentous plant viral nanoparticle Potato virus X. Mol Pharmaceutics. 2013; 10:33–42.
41. Steinmetz NF, Ablack AL, Hickey JL, Ablack J, Manocha B, Mymryk JS, Luyt LG, Lewis JD. Intravital imaging of human prostate cancer using viral nanoparticles targeted to gastrin-releasing Peptide receptors. Small. 2011; 7:1664–1672. [PubMed: 21520408]

42. Destito G, Yeh R, Rae CS, Finn MG, Manchester M. Folic acid-mediated targeting of cowpea mosaic virus particles to tumor cells. Chem Biol. 2007; 14:1152–1162. [PubMed: 17961827]

43. Wu Z, Chen K, Yildiz I, Dirksen A, Fischer R, Dawson PE, Steinmetz NF. Development of viral nanoparticles for efficient intracellular delivery. Nanoscale. 2012; 4:3567–3576. [PubMed: 22508503]

44. Cho CF, Shukla S, Simpson EJ, Steinmetz NF, Luyt LG, Lewis JD. Molecular targeted viral nanoparticles as tools for imaging cancer. Methods Mol Biol. 2014; 1108:211–230. [PubMed: 24243252]

45. Baylis SA, Strijbos PJ, Sandra A, Russell RJ, Rijhsinghani A, Charles IG, Weiner CP. Temporal expression of inducible nitric oxide synthase in mouse and human placenta. Mol Hum Reprod. 1999; 5:277–286. [PubMed: 10333363]

46. Arora S, Olszewski MA, Tsang TM, McDonald RA, Toews GB, Huffnagle GB. Effect of cytokine interplay on macrophage polarization during chronic pulmonary infection with Cryptococcus neoformans. Infect Immun. 2011; 79:1915–1926. [PubMed: 21383052]

47. Hou GQ, Guo C, Song GH, Fang N, Fan WJ, Chen XD, Yuan L, Wang ZQ. Lipopolysaccharide (LPS) promotes osteoclast differentiation and activation by enhancing the MAPK pathway and COX-2 expression in RAW264.7 cells. Int J Mol Med. 2013; 32:503–510. [PubMed: 23740407]

48. Jordans S, Jenko-Kokalj S, Kuhl NM, Tedelind S, Sendt W, Bromme D, Turk D, Brix K. Monitoring compartment-specific substrate cleavage by cathepsins B, K, L, and S at physiological pH and redox conditions. BMC Biochem. 2009; 10:23. [PubMed: 19772638]

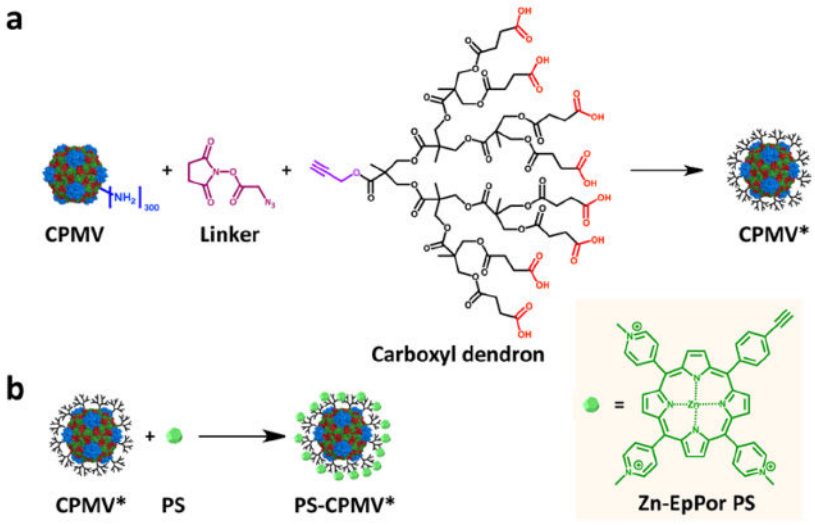

Figure 1.

Schematic of carboxyl dendron conjugation and PS attachment. (a) Alkyne-functionalized carboxyl dendrons were attached to CPMV using an intervening azide linker. (b) Zn-EpPor PS was then incorporated through electrostatic interactions with the dendrons. Structure of PS is shown in inset on right.

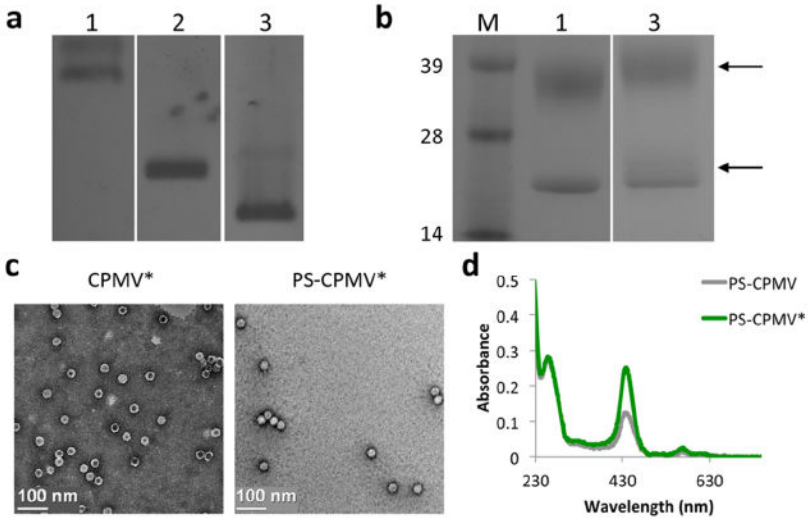

Figure 2.

Characterization of modified particles. (a) Native agarose gel of CPMV, CPMV-N_3, and CPMV* showed expected shifts in band mobility due to increasing negative charge of the modified particles. 1 = CPMV; 2 = CPMV-N_3; 3 = CPMV*. (b) SDS gel electrophoresis revealed additional density (arrows) for CPMV* above the unmodified coat protein bands due to attachment of carboxyl dendrons, with about 45% modification based on densitometric analysis. CPMV consists of 60 copies of a small 24 kDa and a large 42 kDa coat protein. M = SeeBlue Plus2 molecular weight marker. (c) TEM images of CPMV* and PS-CPMV* demonstrates particle integrity after modification. (d) UV/visible spectroscopy of PS-CPMV and PS-CPMV* showed enhanced interaction of PS with CPMV* compared to CPMV.

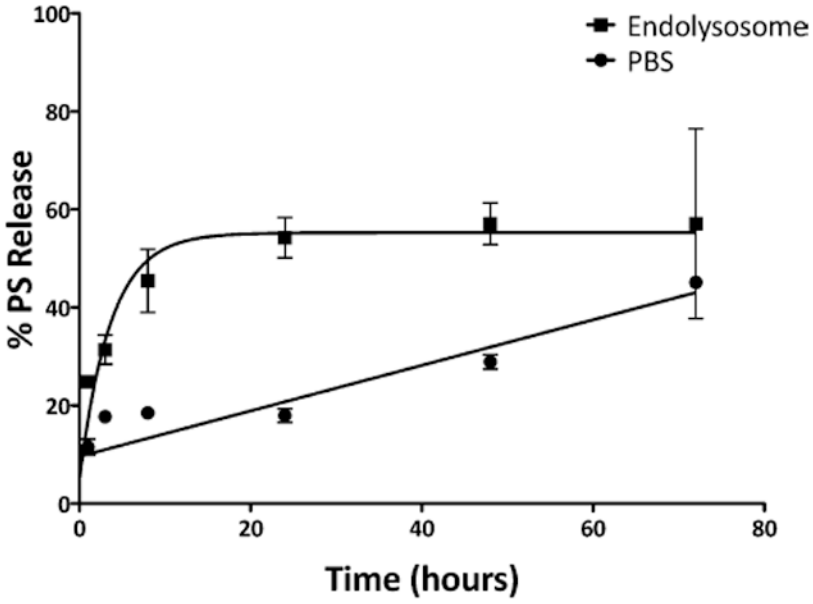

Figure 3.

PS release profile. PS-CPMV* was dialyzed against PBS and endolysosomal buffer (pH 5) at 37 °C using dialysis units with a molecular weight cutoff of 10 kDa. Samples at each time point were analyzed by UV/visible spectroscopy to determine PS concentration. The measurements were performed in triplicate.

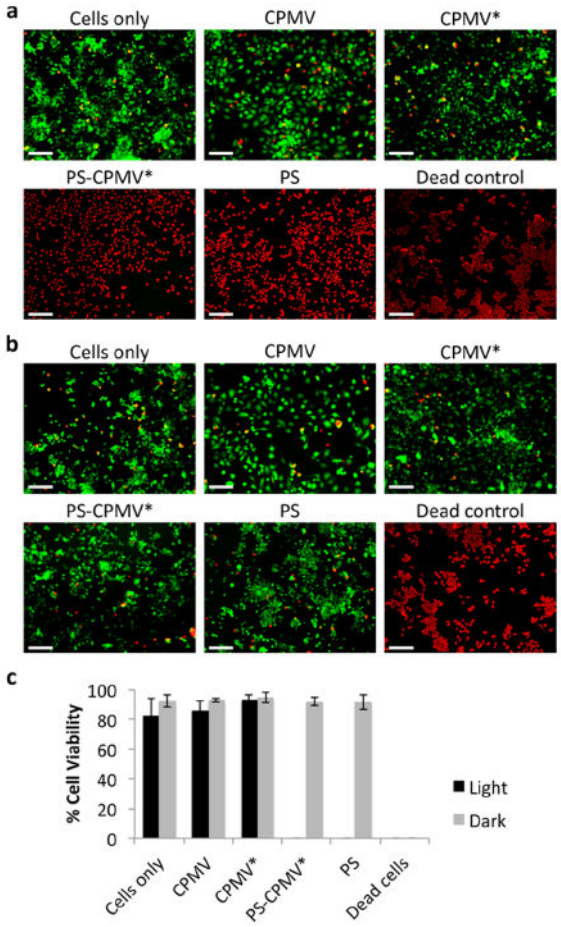

Figure 4.

LIVE/DEAD assay of RAW 264.7 macrophages. (a) Representative images after photodynamic therapy of cells incubated with CPMV, CPMV*, PS-CPMV*, or PS and LIVE/DEAD cell staining. Incubation for 30 min with 70% methanol was utilized as a control for dead cells. Calcein-AM staining of live cells is shown in green, and ethidium homodimer-1 staining of dead cells is shown in red. Scale bar = 200 μm. (b) Dark controls show no cytotoxicity of CPMV formulations or PS alone in the absence of light therapy. Scale bar = 200 μm. (c) Quantification of percentage live cells as measured by ImageJ analysis. Two images for each sample in triplicate were analyzed, and error bars show the standard deviation.

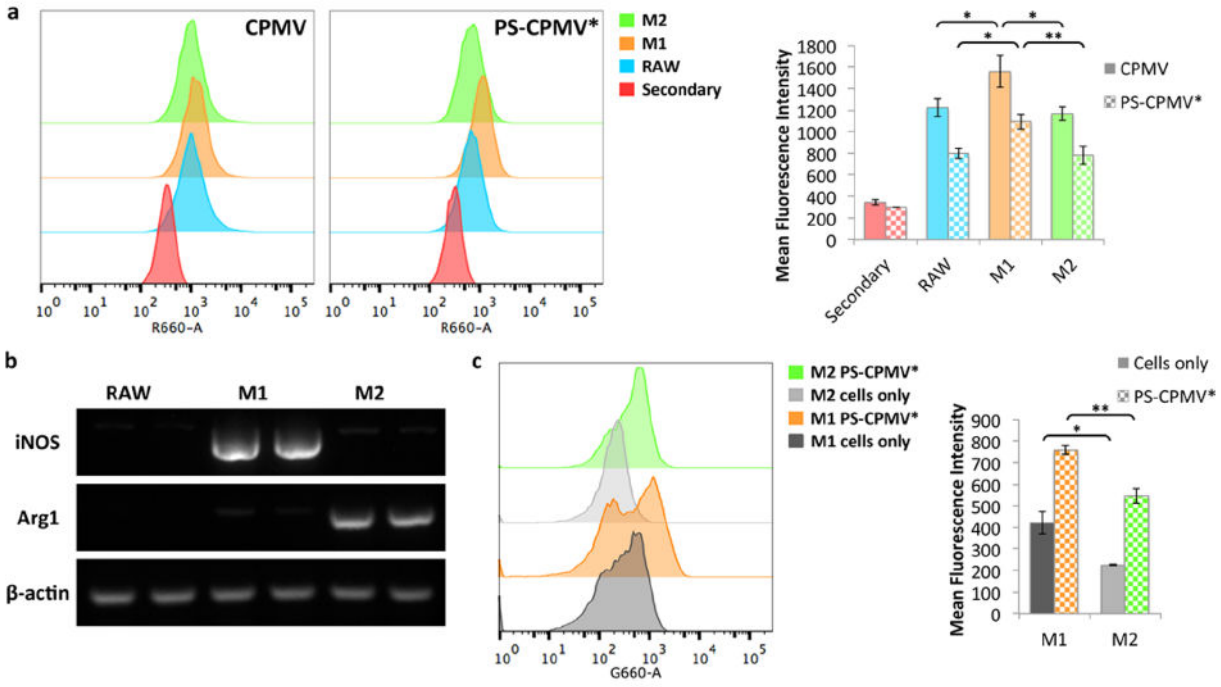

Figure 5.

Macrophage polarization and comparison of CPMV association. (a) Flow cytometry analysis of CPMV and PS-CPMV* association with polarized macrophages show increased signal in M1 macrophages. Particles were stained using a rabbit anti-CPMV antibody followed by a secondary Alexa Fluor 647-labeled anti-rabbit antibody. Secondary only staining was used as the control, with similar results observed for cells without staining. Histograms are shown to the left, and quantification of mean fluorescence intensity is shown to the right. For the bar graphs, data for CPMV are shown as solid bars, while PS-CPMV* data are checkered, and statistical significance is indicated by asterisks (* $p < 0.05$, ** $p < 0.01$). (b) RAW 264.7 macrophage cells were polarized with treatment with either LPS and IFN-γ or IL-4 and verified by RT-PCR analysis for increased iNOS and Arg1 expression for M1 and M2 polarization, respectively. Treatment was performed in duplicate. Untreated cells were analyzed for comparison, and β-actin served as a loading control. (c) Flow cytometry analysis of PS-CPMV* uptake based on PS signal also revealed increased fluorescence in M1 macrophages compared to M2 macrophages. Histograms are shown to the left, and quantification of mean fluorescence intensity is shown to the right. For the bar graphs, cells only data are shown as solid bars, while PS-CPMV* data are checkered. Statistical significance is indicated by asterisks (* $p < 0.05$, ** $p < 0.01$).

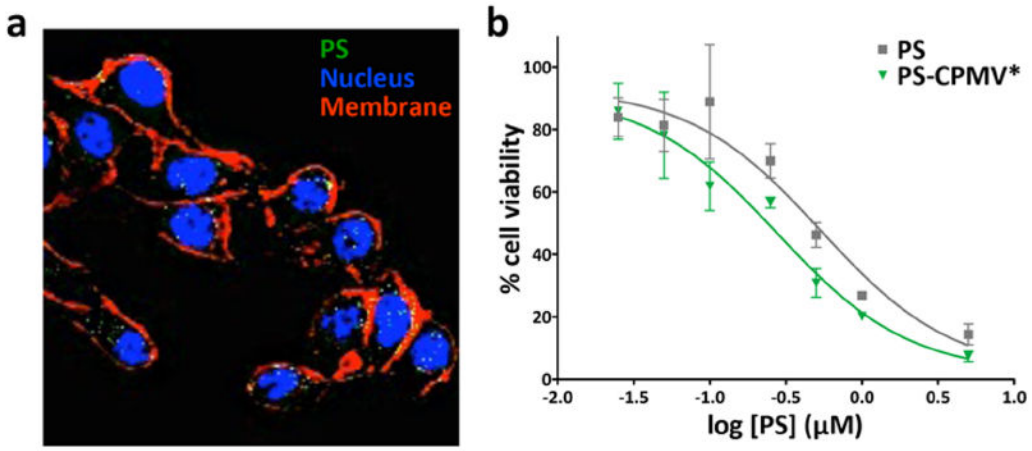

Figure 6.

Uptake and cell killing in B16F10 melanoma cell line. (a) Confocal microscopy of cells incubated with PS-CPMV* showed PS uptake (pseudocolored green). The nucleus is shown in blue (DAPI) and the cell membrane pseudocolored in red (Alexa Fluor 488-labeled WGA). (b) MTT cell viability assay of cells after 8 h of particle uptake and white light illumination for half an hour revealed a slight increase in cell killing efficacy for particulate delivery of PS. Free PS had a IC_{50} of 0.54 μM (data reproduced from ref 21), while PS-CPMV* had an IC_{50} of 0.28 μM.